

Banding Artifact Reduction in Electrophotographic Printers by Using Pulse Width Modulation

Guo-Yau Lin†, Jimmy M. Grice†, Jan P. Allebach†, and George Chiu‡
†School of Electrical and Computer Engineering
‡School of Mechanical Engineering
Purdue University
West Lafayette, IN 47907-1285

Wayne Bradburn and Jeff Weaver
Hewlett-Packard Company
Boise, ID 83706

Abstract

We propose a system to reduce electrophotographic laser printer banding artifacts due to optical photoconductor (OPC) drum velocity fluctuations. The drum velocity fluctuations are sensed with an optical encoder mounted on the drum axis. Based on the line-to-line differential encoder count, we modulate the laser pulse width to compensate fluctuations in development that would otherwise occur. We present an analysis of the system, including the compensation algorithm that determines the desired pulse-width as a function of differential encoder count. Characterization of the system is based on printing, scanning, and processing a special test page that yields information about line-spacing and absorptance fluctuations. This data is synchronized with the encoder count signal that was recorded during the printing of the test page. Finally, we present experimental results for an HP LaserJet 4M printer that demonstrate the efficacy of the system in reducing banding due to OPC drum velocity fluctuations.

1. Introduction

In this paper, we classify as *banding* those artifacts that are due to quasiperiodic fluctuations in process direction parameters. Since no variation in scan direction parameters is involved, the artifacts are constant in the scan direction. With laser printers, banding artifacts are primarily due to fluctuations in the angular velocity of the optical photoconductor (OPC) drum. These fluctuations result in non-uniform line spacing which causes a corresponding fluctuation in developed toner on the printed page.

Banding artifacts have been widely studied and modeled[1, 2, 3, 4]. To reduce banding, one can either design a better mechanical system, or compensate the source of the banding through feedback. To improve the mechanical system, one can use larger diameter gears, which increases the frequencies associated with tooth-to-tooth fluctuations in drive train velocity. This will also increase the angular momentum of the system, which decreases the sensitivity to velocity disturbances. The gear train can also be designed with a coupling mechanism to reduce velocity perturbations[5]. In a similar vein, design methods have been proposed to reduce banding induced by the charger roller[6] and cleaning blade[7].

Feedback systems for banding compensation may be categorized into two groups. In the first group, we have systems that directly compensate the line spacing error via laser beam deflection[8, 9]. In the second group, we have systems that indirectly compensate the line spacing error by varying the laser beam exposure[10, 11, 12, 13]. Both types of systems require a sensor to detect the OPC drum angular velocity.

Among these banding reduction strategies, our work is most closely related to Morrison's invention[12], which uses two interference gratings to obtain the OPC drum velocity, and proposes several means of adjusting the laser beam exposure or moving the laser diode. However, the system model and compensation scheme are not clearly discussed, nor are experimental results presented. In fact, few experimental results for any type of banding reduction strategy have been reported in the literature. In this paper, we present a system that uses laser beam pulse width modulation (PWM) to compensate fluctuations in line spacing. The line spacing information is obtained from an optical encoder mounted on the OPC axis. Our system is based

on a 600 dpi HP LaserJet 4M printer[i]. All the parameters and experimental results presented in this paper are for that printer. This paper is organized as follows. In Sec. 2, we characterize the banding based on measurements from a printed test pattern. Section 3 describes the architecture of the system that we use to reduce banding. Section 4 contains the system analysis. In Sec. 5, we present experimental results. Finally, in Sec. 6, we draw some conlusions from our work.

2. Test Pattern Design and Analysis

To measure banding, we print a specially designed test page, then scan it, and analyze the scanned data. The test page is designed to show banding in the process direction and to also yield information about the scan line positions in the process direction.

2.1. Test Pattern Design

Figure 1 shows that the test pattern is separated into three vertical components. Along the left and right edges are a series of registration marks to establish the position of each scan line. These registration marks are staggered from line-to-line to permit segmentation of the individual registration marks and to eliminate the interaction between the exposure of the marks on adjacent lines. Placing the marks symmetrically on either side of the page facilitates correction of skew due to misalignment of the printed page on the scanner drum.

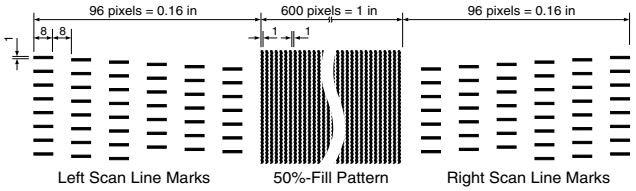

Figure 1: *Layout of the test pattern. Banding is measured from the center 50%-fill pattern. The registration marks on either side are used to determine scan line position.*

The center region of the test pattern is used to measure the effect of the line spacing fluctuation on printed absorptance. Since banding is most apparent in flat midtone areas, we design a 50%-fill test pattern as shown in Fig. 1 to measure it. In this 50%-fill test pattern, we print a vertical line at every other column of addressable pixels. Compared with any other 50%-fill pattern, this gives us the maximum spatial resolution of banding.

2.2. Test Pattern Analysis

After printing the test pattern, the next step is to extract the information from the print by scanning it on a high resolution drum scanner[ii] at 2000 dpi. Figure 2 shows the scanned test pattern. First we segment the registration marks on the scanned image, and compute their centroids $y_{_L}(n)$ and $y_{_R}(n)$ along the process direction. We average these values to obtain our estimate $y(n) = \frac{1}{2}[y_{_L}(n) + y_{_R}(n)]$ of the position of the n-th line, and then compute the line spacing as $d_y(n) = y(n) - y(n-1)$.

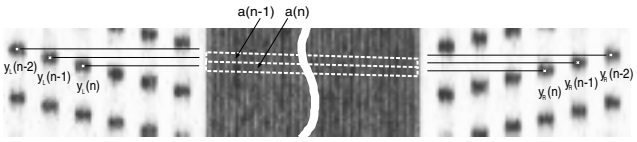

Figure 2: *Test pattern scanned at 2000 dpi. For clearer illustration, the image is expanded 4 times in the process direction. The one dimensional absorptance signal $a(n)$ is computed by averaging the image data between the dashed lines. The coordinates of these lines are determined with the help of the corresponding scan line registration marks.*

With the help of the coordinates of the corresponding registration marks, we segment the scanned absorptance test pattern into cells indicated by the dashed lines shown in Fig. 2. We then average the absorptance within each cell to obtain the absorptance sequence $a(n)$. We will refer to this as the *projected* absorptance. Figures 3a and 3b show the signal waveforms for the scan line spacing $d_y(n)$ and absorptance $a(n)$. In these figures, we also show the spectra for $d_y(n)$ and $a(n)$. In both spectra, we observe the same main peaks at 8.6, 12.8, and 33.1 cycles/in. The absorptance spectrum contains additional very low frequency energy that is not present in the spectrum of the line spacing data. This energy is due to disturbances in the paper path that occur after writing the latent image on the OPC. Conversely, the line spacing spectrum contains high frequency energy not present in the absorptance spectrum. We believe that this energy is due to errors in estimating the centroids of the scan line registration marks.

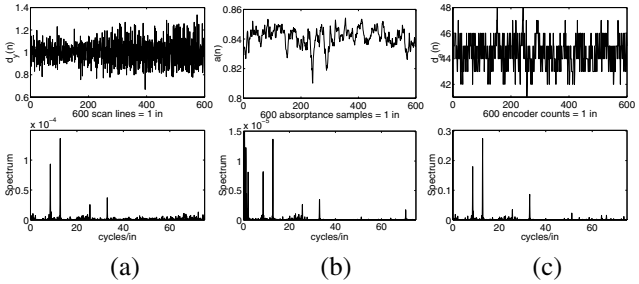

Figure 3: *Waveforms and spectra of (a) scan line spacing $d_y(n)$, (b) projected absorptance $a(n)$, (c) encoder count between scan lines $d_e(n)$. The same major banding frequencies are observed in all three signals.*

[i] HP LJ4M: Hewlett-Packard Company, Boise, ID 83706.

[ii] Howtek Scanmaster D4000: Howtek, Inc., Hudson, NH 03051.

3. Banding Reduction System

Our basic strategy for banding reduction is to modulate the laser beam exposure time according to the variations in the scan line spacing. In this section, we discuss how laser beam exposure is controlled by pulse width modulation (PWM); and we describe the banding reduction system architecture.

3.1. Laser Beam Pulse Width Modulation

To control exposure, one can either adjust the input voltage to the laser beam (amplitude modulation), or adjust the duration of the laser pulses (pulse width modulation or PWM). Here we use PWM which provides the capability to switch the laser beam on and then off at fractional positions within a nominal printer-addressable pixel. In our system, the turned-on portion is always centered in the pixel.

In the absence of PWM, the locally averaged absorptance will depend on the bit map sent to the marking engine. For a fixed bit map, the locally averaged absorptance will increase with increasing pulse width p. However, this relationship is generally not linear and may also depend on the bit map itself. In our work, we ignore the dependence on the bit map, and base the banding compensation system on a single relation for average absorptance as a function of pulse width p. We obtain this relation by printing the test page described in Sec. 2.1 for different fixed values of p, and processing it as described in Sec. 2.2 to obtain absorptance, which in this case, we average over the entire 50%-fill region on the page. We will refer to this as the *average* absorptance.

Figure 4 shows the resulting curve for average absorptance $a_0(p)$ as a function of pulse width p. We see that for $0.0 \leq p \leq 0.3$, there is very little development. Then as p increases from 0.4 to 0.6, the absorptance increases very rapidly to approximately 80% of its maximum value. Beyond $p = 0.7$, the absorptance increases more slowly to its maximum value of 0.84. While modulating pulse width to compensate banding, we want to operate with as large an average value of p as possible, since this corresponds to the maximum average absorptance that we can print in solid black areas of the page. Thus, we will want to confine our range of operation to $0.7 \leq p \leq 1.0$. Over this range, the average absorptance can be approximated well as a linear function of pulse width:

$$a_0(p) = \alpha p + \beta, \quad 0.7 \leq p \leq 1.0, \tag{1}$$

where $\alpha = 0.417$ and $\beta = 0.424$.

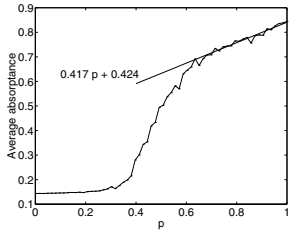

Figure 4: *Average absorptance a_0 as a function of pulse width p. For $p \in [0.7, 1]$, we approximate this relation by a linear function as shown.*

3.2. System Architecture

Figure 5 shows a block diagram of our system for banding reduction. A Canon M1 optical encoder[iii] is mounted on the OPC drum axis. This digital encoder generates $100,000$ counts per revolution when operated in double resolution mode. Since the OPC drum circumference is 3.71 in, this corresponds to 44.92 counts per $1/600$ inch nominal scan line interval. However, the speed of the drive motors of the OPC drum and the polygon mirror may vary slightly from engine to engine. Due to this fact, the actual nominal counts between two scan lines are 44.5 in our experimental setup.

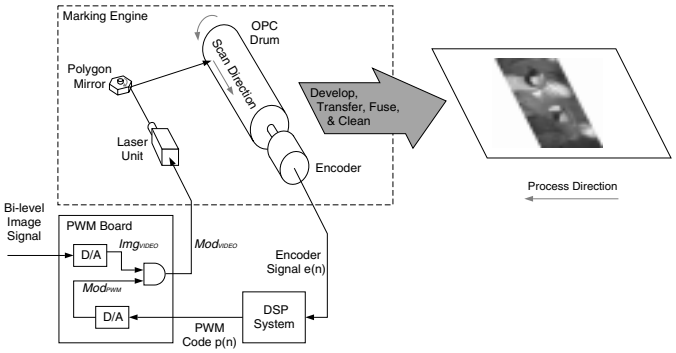

Figure 5: *Block diagram of the banding reduction system. An optical encoder is mounted on the OPC drum axis in order to track the speed of the OPC drum. The DSP system computes the PWM code needed for each scan line according to the encoder output. The PWM system modulates the bi-level image signal according to the PWM code.*

When the laser beam reaches the left edge of the OPC drum, a beam detect signal is generated. This signal triggers the sampling of the optical encoder output to provide an encoder count for the current scan line. This information is used to generate a pulse width $p(n)$ for the current line, which is kept constant across it. This pulse width must be computed before the laser beam reaches the first addressable pixel on the OPC drum, which is a distance of

[iii] Canon Laser Rotary Encoder M1: Canon, Inc., Tokyo 146-8501, Japan.

0.125 in from the point at which the beam detect signal is generated. Since the laser beam is traveling at a velocity of 9.44×10^3 in/s across the page, we have 13.2 μs to perform this calculation. In our prototype system, the PWM code is computed with a Motorola DSP56002EVM evaluation board[iv] based on the DSP56002 DSP chip. This chip is a fixed point processor which runs at a clock speed of 80 MHz. At this rate, we can execute 528 instructions to compute the pulse width code, which is an 8 bit value. The most significant 2 bits are used to encode the justification mode; and the least significant 6 bits carry the pulse width information. Here we only use center justification so the most significant 2 bits are set to 0.

The PWM board converts the bi-level digital image signal to an analog video signal Img_{VIDEO}. Running on the same clock, a piggyback board on the PWM board converts the 8 bit PWM code to an analog modulation waveform Mod_{PWM}. The signal Mod_{PWM} is synchronized to Img_{VIDEO} by the laser beam detect pulses, which trigger the DSP system to generate the PWM code line-by-line. Finally, Img_{VIDEO} is AND-ed with Mod_{PWM} as illustrated in Fig. 6, on the piggyback board to generate the modulated video signal Mod_{VIDEO} sent to the laser.

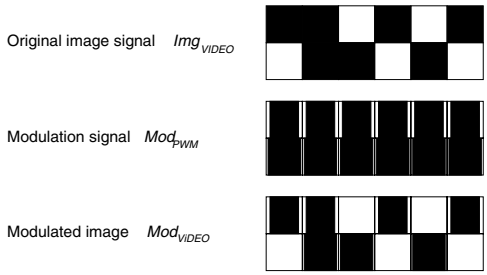

Figure 6: Original halftone image signal, pulse width modulation signal, and resulting modulated image signal. The modulated image is the AND of the original bi-level image signal and the pulse width modulation signal. In the compensation system, we use a fixed pulse width for each scan line.

3.3. Relation between Encoder Signal and Absorptance Signal

In Sec. 2.2, we printed a specially designed test pattern to determine the relation between line-spacing and printed absorptance. In order to develop our compensation algorithm, we need the corresponding relation between encoder count and printed absorptance. We can print the same test pattern as before, and record the encoder count sequence $e(n)$ while the page is being printed. However, we need a way to synchronize the encoder count with the measured absorptance sequence $a(n)$. To do this, we again use the beam detect signal which generates a count that is incremented by one at the start of each line. When the beam detect count reaches a specified value, we initiate sampling of the encoder output and at the same time set the pulse width p equal to 0 for several lines. This generates a clearly identifiable white gap in the test pattern that tells us where to start the sequence $a(n)$ when we analyze the printed test page.

Figure 3c shows the differential encoder signal

$$d_e(n) = e(n) - e(n-1), \tag{2}$$

corresponding to the line spacing and absorptance signals obtained from the printed test pattern. As mentioned earlier, the nominal value for this signal is $d_e^0 = 44.5$. Figure 3c also shows the spectrum of this signal. We see that it too contains the same major spectral peaks as the line spacing and absorptance signals. However, it lacks both the low frequency content of the absorptance signal and the high frequency content of the line spacing signal.

To establish the relation between the encoder perturbation

$$\delta_e(n) = d_e(n) - d_e^0, \tag{3}$$

and the projected absorptance perturbation

$$\delta_a(n) = a(n) - a_0, \tag{4}$$

we use a scatter plot as shown in Fig. 7a. By applying a bandpass filter to extract the spectral peak at 8.6 cycle/in, we see a linear relation between these two signals. We can think of the slope of the line in Fig. 7a as a measure of the efficiency of perturbations in line spacing in generating perturbations in absorptance, i.e. banding. It is reasonable to expect that the slope in Fig. 7a will depend on pulse width p, since banding depends on the average absorptance a_0 as well. Thus we have

$$\delta_a(n) = \eta(p)\delta_e(n). \tag{5}$$

By again printing and processing the test pattern for different values of p, we can determine the efficiency function $\eta(p)$ which is shown in Fig. 7b. We see that the banding efficiency $|\eta(p)|$ decreases with increasing p over the range of values of p that are of interest, and this relation can be modeled well as a linear function of p:

$$\eta(p) = \zeta p + \tau, \quad 0.7 \le p \le 1.0. \tag{6}$$

Here $\zeta = 0.039$ and $\tau = -0.045$ are calculated from Fig. 7b by a least-squares fit to the data.

4. System Analysis

4.1. Compensation Algorithm

Having specified the system architecture and characterized the relation between all of its components in the preceding

[iv] DSP56002EVM: Motorola, Inc., Motorola Literature Distribution, P.O. Box 5405, Denver, Colorado 80217.

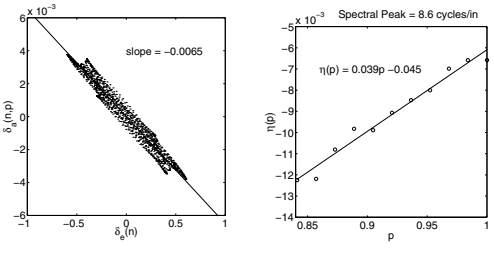

(a) (b)

Figure 7: *(a) Scatter plot of the absorptance perturbation $\delta_a(n)$ vs. encoder count perturbation $\delta_e(n)$ with $p = 1$. The perturbation signals are obtained by bandpass filtering to $[7, 10]$ cycles/in. (b) Banding efficiency $\eta(p)$ for the spectral peak at 8.6 cycles/in.*

two sections, we are now ready to derive the compensation algorithm itself. It will specify the desired pulse width p as a function of the differential encoder count d_e to suppress banding. We start by writing the projected absorptance signal as the sum of its nominal value and a perturbation term caused by the OPC drum velocity fluctuations

$$a(n) = a_0(p) + \delta_a(n, p). \tag{7}$$

Both these terms depend on pulse width p.

To cancel the perturbation and obtain a fixed $a(n) = a_0(p_0)$, where p_0 is the nominal pulse width, we vary p as a function of n. Therefore, Eq. (7) becomes

$$a_0(p_0) = a_0(p(n)) + \delta_a(n, p(n)). \tag{8}$$

Replacing $a_0(\cdot)$ by the linear model in Eq. (1) and rearranging, we obtain

$$\begin{aligned} \alpha p_0 + \beta &= \alpha p(n) + \beta + \delta_a(n, p(n)), \\ p(n) &= p_0 - \frac{1}{\alpha}\delta_a(n, p(n)). \end{aligned} \tag{9}$$

Next, we replace $\delta_a(n, p(n))$ by Eq. (5) to yield

$$p(n) = p_0 - \frac{1}{\alpha}\eta(p(n))\delta_e(n). \tag{10}$$

Finally, we apply the banding efficiency function from Eq. (6), and rearrange again to obtain

$$\begin{aligned} p(n) &= p_0 - \frac{1}{\alpha}(\zeta p(n) + \tau)\delta_e(n), \\ p(n) = \frac{p_0 - \frac{\tau}{\alpha}\delta_e(n)}{1 + \frac{\zeta}{\alpha}\delta_e(n)} &= \frac{p_0 - \frac{\tau}{\alpha}(d_e(n) - d_e^0)}{1 + \frac{\zeta}{\alpha}(d_e(n) - d_e^0)}. \end{aligned} \tag{11}$$

As discussed in Sec. 3.1, we want to choose as large a value of p_0 as possible. From Fig. 3c, we observe that the differential encoder count $d_e(n)$ varies between 41 and 48. The pulse width $p(n)$ will take on its maximum value when $d_e(n)$ is largest, because this is when the scan lines are farthest apart, resulting in the greatest drop in absorptance $a(n)$ in the absence of compensation. Since the pulse width cannot exceed 1, we substitute $p(n) = 1$ and $d_e(n) = 48$ into Eq. (11) and solve for p_0 to obtain $p_0 = 0.933$.

Figure 8 shows $p(n)$ as a function of the differential encoder signal $d_e(n)$ for this value of p_0. Since our PWM system has only 6 bits for pulse width, $p(n)$ has to be quantized to 64 levels as indicated in Fig. 8 by the sample points.

Following the approach used for the spectral peak at 8.6 cycles/in to process other spectral peaks, we find that ζ and τ vary little for different peaks. Thus, in the interest of simplicity, we use the same set of values for ζ and τ.

For efficient implementation, we precompute Eq. (11) for the differential encoder counts between 41 and 48, and store these pulse widths as a look-up table in the DSP system. In the DSP system, the computation of subtracting the previous encoder count from the current count and performing the table look-up can be done in 10 instructions. This is far fewer than the system constraint of 528 instructions discussed in Sec. 3.2.

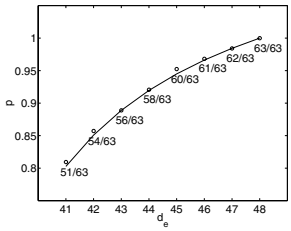

Figure 8: *PWM code as a function of differential encoder signal $d_e(n)$.*

5. Experimental Results

Figure 9 shows the scanned 50%-fill test pattern and a halftone image both printed without and with banding reduction. Comparing them, we see that the banding artifacts are significantly reduced. Figure 10 shows the spectra of the projected absorptance of the 50%-fill pattern without and with banding reduction. To better illustrate the visual significance of these results, we also show the spectra weighted by the contrast sensitivity function[14] of the human viewer. We observe that the main spatial frequency peaks are suppressed after banding reduction. However, we still see the low frequency components and also a peak at 70 cycles/inch. Those frequency components are induced outside of the OPC drum and cannot be detected by the encoder. To suppress them, we would need to have other sensors to acquire the information from the perturbation sources.

6. Conclusion

Banding is an important artifact for EP printers. It is primarily caused by fluctuations in the OPC drum velocity.

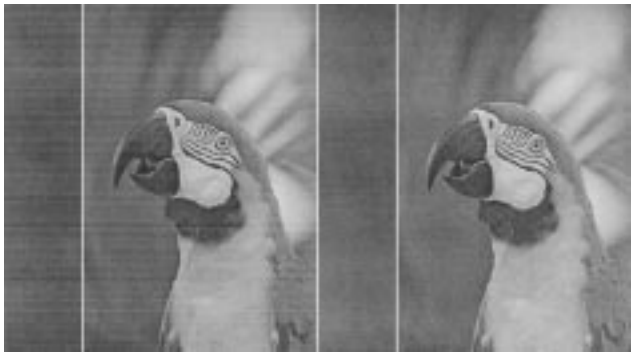

Figure 9: *Portion of printed images (3 inch high) scanned at 150 dpi. From the left,* 50%*-fill test pattern and a halftone image both printed without banding reduction, and the same images printed with banding reduction.*

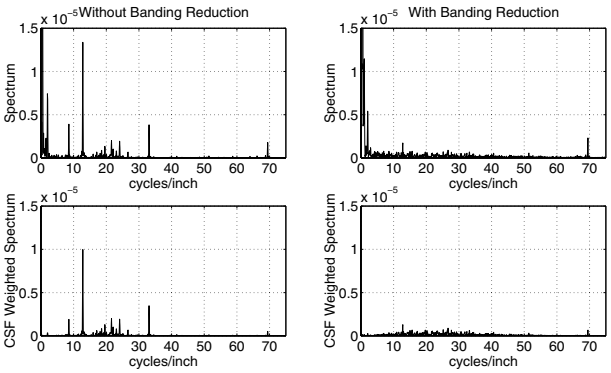

Figure 10: *Spectra unweighted (top row) and weighted by the contrast sensitivity function*[14] *(bottom row) for the human viewer (15 in viewing distance) (a) without, and (b) with banding reduction. In (b), the low frequencies and the peak at 70 cycles/in are not compensated because the encoder cannot detect those banding sources.*

These fluctuations result in variations in line spacing, causing excessive development if the line spacing is too small, and too little development if the line spacing is too large. We have proposed a system for reducing banding that is based on sensing the OPC drum velocity fluctuations with an optical encoder mounted on the drum shaft. We then modulate the laser beam pulse width line-by-line to compensate for the impact of line-spacing errors on development.

Our experimental results show that the method suppresses very well the banding due to fluctuations in OPC drum velocity. However, lower frequency banding due to other sources in the printer is not suppressed. Suppression of banding at these frequencies would require additional sensors to capture the sources of the low frequency fluctuation. Although we have not demonstrated it in this system, we believe that our compensation algorithm can be modified for use in a system in which it is desired to exploit pulse width modulation both as part of the halftoning algorithm and to suppress banding.

Acknowledgment

The authors would like to thank Farhan Baqai for his contribution to the design of the test pattern.

References

1. P. Burns, M. Rabbani, and L. Ray, "Analysis of image noise due to position errors in laser writers," *Applied Optics*, vol. 25, no. 13, pp. 2158–68, 1986.
2. P. Melnychuk and R. Shaw, "Fourier spectra of digital halftone images containing dot-position errors," *J. Opt. Soc. Am.*, vol. 5, no. 8, pp. 1328–38, 1988.
3. D. Haas, "Contrast modulation in halftone images produced by vibration in scanline spacing," *Journal of Imaging Technology*, vol. 15, pp. 48–55, 1989.
4. R. Loce, W. Lama, and M. Maltz, "Modeling vibration-induced halftone banding in a xerographic laser printer," *Journal of Electronic Imaging*, vol. 4(1), pp. 8–61, 1995.
5. P. Jeran, "Gear train control system for reducing velocity induced image defects in printers and copiers," *U.S. Patent 5,812,183 assigned to Hewlett-Packard Company*, 1998.
6. H. Kawamoto, K. Udagawa, and M. Mori, "Vibration and noise induced by electrostatic force on a contact charger roller of electrophotography," *Journal of Imaging Science and Technology*, vol. 39, pp. 477–480, 1995.
7. H. Kawamoto, "Chatter vibration of a cleaner blade in electrophotography," *Journal of Imaging Science and Technology*, vol. 40, pp. 8–13, 1996.
8. W. Foote and R. Sevier, "Laser printer with apparatus to reduce banding by servo adjustment of a scanned laser beam," *U.S. Patent 5,760,817 assigned to Hewlett-Packard Company*, 1998.
9. R. Lawton and D. Marshall, "Beam deflecting for resolution enhancement and banding reduction in a laser printer," *U.S. Patent 5,920,336 assigned to Hewlett-Packard Company*, 1999.
10. W. Lama, R. Loce, and J. Durbin, "Image bar printer compensated for vibration-generated scan line errors," *U.S. Patent 4,801,978 assigned to Xerox Company*, 1989.
11. R. Loce and W. Lama, "Halftone banding due to vibrations in a xerographic image bar printer," *Journal of Imaging Technology*, vol. 16(1), pp. 6–11, 1990.
12. R. Morrison, "System and method for modifying an output image signal to compensate for drum velocity variations in a laser printer," *U.S. Patent 5,729,277 assigned to Hewlett-Packard Company*, 1998.
13. D. Costanza, R. Jodoin, and R. Loce, "Method and apparatus for compensating for raster position errors in output scanners," *U.S. Patent 5,900,901 assigned to Xerox Company*, 1999.
14. R. Näsänen, "Visibility of halftone dot textures," *IEEE Transactions on Systems, Man, and Cybernetics*, vol. SMC-14, no. 6, pp. 920–924, 1984.

Biography

Guo-Yau Lin received his BS degree in mechanical engineering from the National Taiwan University, Taiwan in 1993, and received MENG degrees both in mechanical and aerospace engineering, and in electrical engineering from Cornell University in 1996 and 1997, respectively. He started his PhD study at Penn State University and is now pursuing his PhD degree in the school of electrical and computer engineering at Purdue University.